Ordered nanoparticle arrays formed on engineered chaperonin protein templates

R. ANDREW MCMILLAN*[1], CHAD D. PAAVOLA[1], JEANIE HOWARD[2], SUZANNE L. CHAN[2], NESTOR J. ZALUZEC[3] AND JONATHAN D. TRENT*[1]

[1]NASA Ames Research Center, Center for Nanotechnology and Astrobiology Technology Branch, Mail Stop 239-15, Moffett Field, California 94035, USA
[2]SETI Institute, 2035 Landings Drive, Mountain View, California 94043, USA
[3]Argonne National Laboratory, Materials Science Division, 9700 South Cass Avenue, Argonne, Illinois 60439, USA
*e-mail: amcmillan@mail.arc.nasa.gov; jtrent@mail.arc.nasa.gov

Published online: 24 November 2002; doi:10.1038/nmat775

Traditional methods for fabricating nanoscale arrays are usually based on lithographic techniques. Alternative new approaches rely on the use of nanoscale templates made of synthetic or biological materials. Some proteins, for example, have been used to form ordered two-dimensional arrays. Here, we fabricated nanoscale ordered arrays of metal and semiconductor quantum dots by binding preformed nanoparticles onto crystalline protein templates made from genetically engineered hollow double-ring structures called chaperonins. Using structural information as a guide, a thermostable recombinant chaperonin subunit was modified to assemble into chaperonins with either 3 nm or 9 nm apical pores surrounded by chemically reactive thiols. These engineered chaperonins were crystallized into two-dimensional templates up to 20 μm in diameter. The periodic solvent-exposed thiols within these crystalline templates were used to size-selectively bind and organize either gold (1.4, 5 or 10 nm) or CdSe–ZnS semiconductor (4.5 nm) quantum dots into arrays. The order within the arrays was defined by the lattice of the underlying protein crystal. By combining the self-assembling properties of chaperonins with mutations guided by structural modelling, we demonstrate that quantum dots can be manipulated using modified chaperonins and organized into arrays for use in next-generation electronic and photonic devices.

The controlled organization of inorganic materials into multi-dimensional addressable arrays is the foundation for both logic and memory devices, as well as other nonlinear optical and sensing devices[1,2]. Many of these devices are currently fabricated using lithographic patterning processes that have progressively developed towards greater integration densities and smaller sizes. At sub-micrometre scales, however, conventional lithographic processes are approaching their practical and theoretical limits. At scales below 100 nm, ion and electron beam lithography becomes prohibitively expensive and time consuming, and more importantly, at these scales quantum effects fundamentally change the properties of devices[3]. While there are strong incentives to develop nanoscale architectures, these developments will require alternative fabrication methods and new insights into the behaviour of materials on nanometre scales [4].

Arrays of nanoparticles formed by non-conventional methods are being explored for use as viable alternatives to standard lithographically patterned devices, and individual nanoparticles, also known as quantum dots (QDs), have been shown to behave as isolated device components such as single-electron transistors[5,6]. Theoreticians have postulated that two-dimensional (2D) arrays of QDs with nanoscale resolution will form the basis of future generations of electronic and photonic devices. The function of these devices will be based on phenomena such as coulomb charging, inter-dot quantum tunnelling and other coherent properties derived from the electronic consequences of confinement and the ratios of nanoparticle surface area to volume[7–10].

Nanoscale templates for constrained synthesis, *in situ* deposition, or direct patterning of nanometre-scale inorganic arrays are being developed using both artificial and natural materials. Artificial materials such as microphase-separated block copolymers[11] and hexagonally close-packed spheres[12] have been used for nanoscale fabrication. Natural materials such as DNA[13,14], bacterial and archaeal surface layer proteins[15–17], virus capsids[18–21], phage[22] and some globular proteins[23] have been used as templates and in other nanoscale applications.

Biomolecules in general are capable of self-assembling into a wide diversity of structures with nanoscale architecture. Proteins in particular can form intricate structures that can be readily manipulated and functionalized because their synthesis is genetically directed. By genetically engineering a protein that, in the presence of adenosine triphosphate (ATP) and Mg^{2+}, self-assembles into regular double-ring structures known as chaperonins, we demonstrate that chaperonins can direct the organization of preformed metal and semiconductor nanoparticle QDs into ordered arrays.

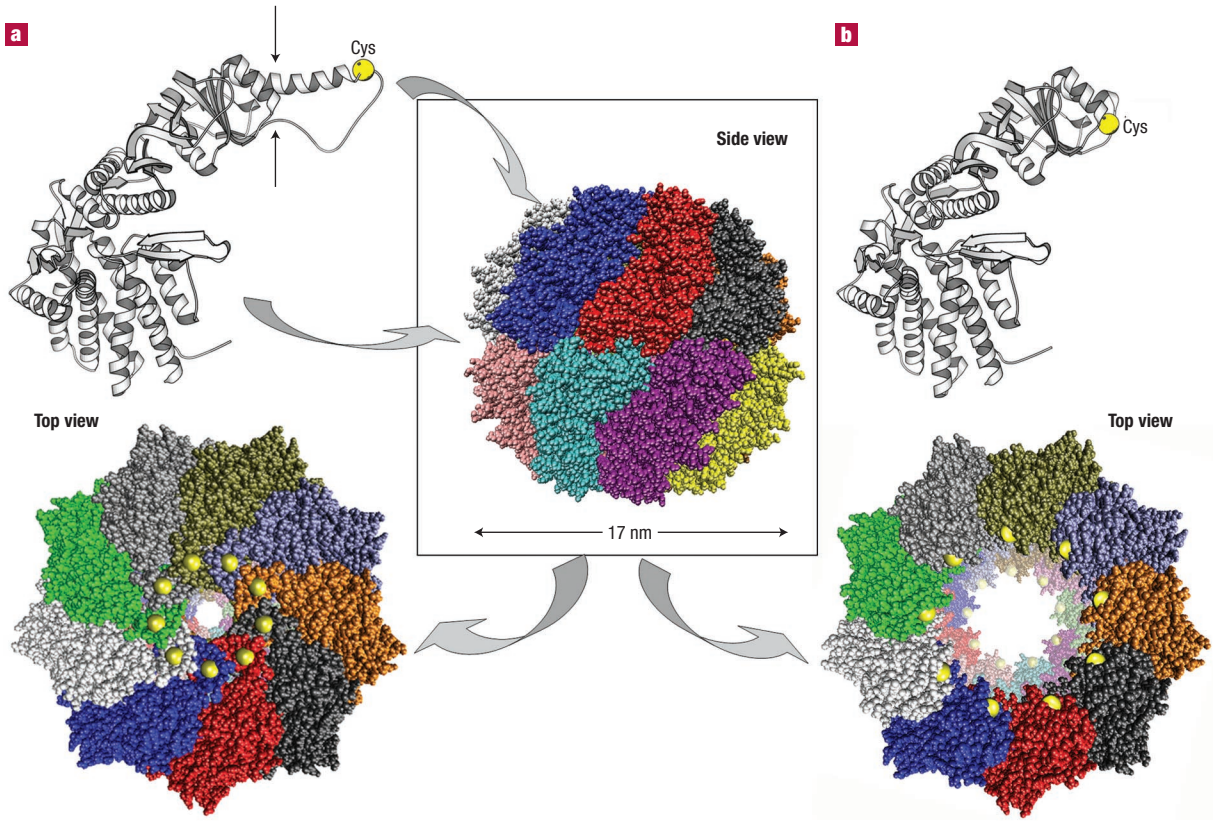

Figure 1 Models depicting the assembly of engineered *S. shibatae* HSP60s into chaperonin variants. **a**, Top: Model of a mutated HSP60 beta subunit indicating apical loop cysteine (Cys) placement in yellow. Bottom: Top view of beta chaperonin variant (with apical loops) revealing the 3-nm pore ringed by nine cysteines indicated in yellow. **b**, Top: Result of genetic removal of the 28 residue apical loop of beta and substitution of cysteine at the site fusing the α-carbon backbone. Genetic modifications were made based on the model in **a** at the positions indicated by the arrows. Bottom: Top-view of loopless chaperonin variant with a 9 nm pore ringed by cysteines. The centre shows a side view of two stacked symmetrical nine-membered rings assembled from mutated beta subunits consistent with both classes of chaperonin variants.

In nature, chaperonins are ubiquitous and essential subcellular structures composed of 14, 16, or 18 subunits called heat shock proteins (HSP60)[24]. These 60-kDa subunits are arranged as two stacked rings 16 to 18 nm tall by 15 to 17 nm wide, depending on their species of origin. We used one of the three HSP60 subunits (beta) from *Sulfolobus shibatae*, an organism that lives in geothermal hot-springs and grows at temperatures of up to 85 °C at pH 2.0. The chaperonins in *S. shibatae* are octadecameric with nine subunits per ring. We chose the beta subunit because: (1) its thermostability makes it easy to purify as a recombinant protein, (2) sequence and structural information are available to guide genetic manipulations, and (3) most importantly, it has been shown to assemble into chaperonins that can assume higher-order structures such as 2D crystals[25,26].

The purification of the beta subunit expressed in *Escherichia coli* involves heating total cell extracts to 85 °C for 30 minutes; this precipitates most *E. coli* proteins, but the thermostable beta remains soluble. Therefore, heating and centrifuging cell extracts separates beta from most *E. coli* proteins, which simplifies further purification using ion exchange chromatography[27].

Guided by structural information, we genetically modified beta to add chemically reactive sites without destroying its ability to assemble into chaperonins and 2D crystals. Although a detailed 3D structure of *S. shibatae* beta is not known, X-ray structures for homologous chaperonin subunits are known[28,29] and detailed transmission electron microscopic (TEM) and cryo-electron microscopic (cryo-EM) analyses of *S. shibatae* chaperonins have been reported[30,31]. Using X-ray structures of homologous subunits and TEM analyses of *Sulfolobus* chaperonins, we produced a hypothetical 3D model for the beta chaperonin[32–34]. We used this model to guide our genetic manipulations. Using the polymerase chain reaction for site-directed mutagenesis, we created two classes of beta mutants, both of which retained their ability to assemble into chaperonins that form 2D crystals (Fig. 1).

In both classes of beta mutants, we changed the single native cysteine residue in beta to a non-reactive alanine to prevent potential problems with folding and with assembly of mutant subunits. We then placed cysteine at different solvent-exposed sites. The thiols of these cysteines provide binding sites for soft metals including gold and zinc. In one class of beta mutants, the exposed cysteine was placed near the tip of a loop of 28 amino acids on the apical domain of beta, which in the assembled chaperonin protrudes into the central cavity. This mutant chaperonin has a ring of reactive thiols with a diameter of approximately 3 nm on both ends (Fig. 1a). In the other class of beta mutants, we removed the protruding 28-amino-acid loop and placed the exposed cysteine on the apical domain itself. The mutant chaperonin assembled from this subunit has a ring of reactive thiols with a diameter of approximately 9 nm and an open pore into its central cavity (Fig. 1b).

The beta subunit proved to have sufficient structural plasticity in its apical domain to accommodate both the amino acid substitutions and deletions we made without losing its ability to form chaperonins and 2D crystals. Under reducing conditions, both classes of beta mutants

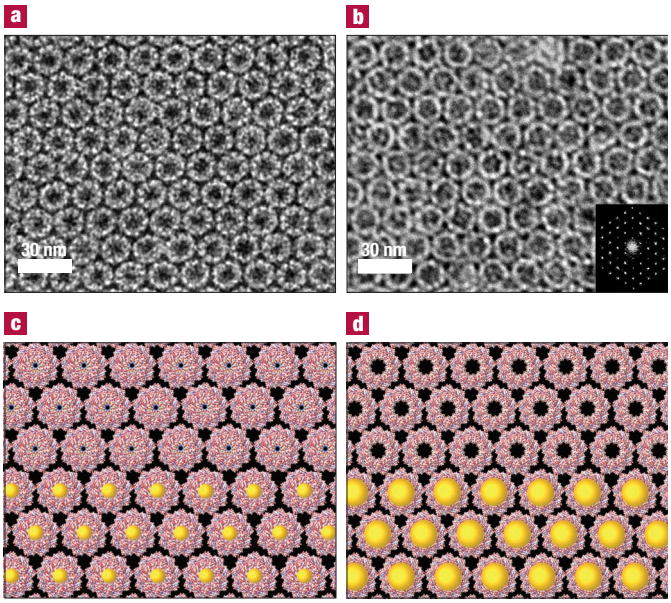

Figure 2 2D crystals of engineered chaperonins as quantum dot array templates. **a**, TEM image of a negatively stained 2D crystal of the beta chaperonin variant with cysteine substitutions at the apical pores. The two-sided-plane group p312 was assigned to the lattice through image analyses of micrographs of *S. shibatae* beta chaperonin 2D crystals[30]. **b**, 2D crystal of the loopless chaperonin variant reveals an apparent increase in pore size (from 3 to 9 nm) as changes in electron density within the pores of the negatively stained rings. Samples in both **a** and **b** were imaged at the same condenser defocus setting. The ordering of the crystal is illustrated in the inset of **b** by the fast Fourier transformation of the image. **c**, A graphical representation of 5 nm gold particles binding within the 3 nm pores of engineered chaperonin 2D crystals, and **d**, 10 nm gold particles binding within the 9 nm pores .

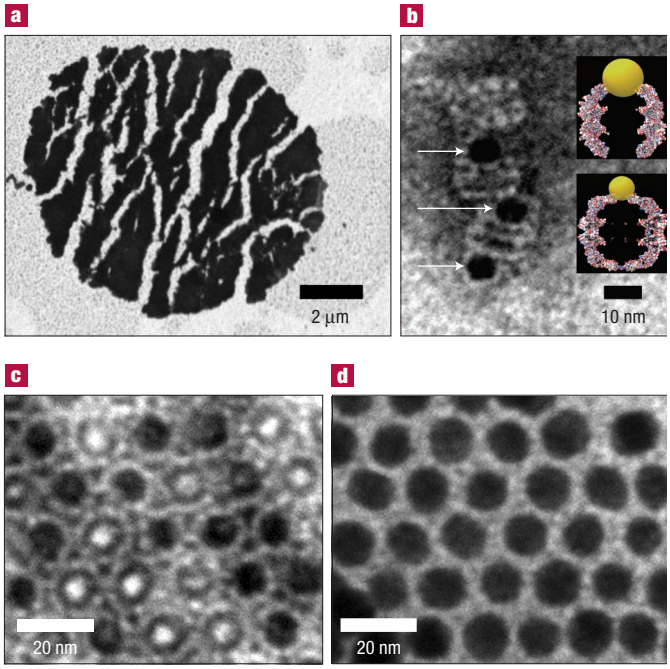

Figure 3 Gold QD binding to engineered chaperonins and chaperonin-templates. **a**, Low-magnification TEM image of 10 μm diameter 2D crystal of the 9-nm-pore chaperonin variant with bound 10 nm gold QDs. The image contrast is from gold QDs bound to the crystalline lattice of the underlying protein template. Drying causes significant sample cracking and contributes to distortions and separation of regions of order within the array. **b**, Higher-magnification stained TEM image of side views of 5 nm gold QDs (arrowed) tethered at the apical pores of the 3-nm-pore mutant chaperonins. Inset: Slab-view cutaway diagrams of postulated orientation of 5 and 10 nm gold QDs bound at the apical pores of the two chaperonin variants. **c**, Stained image of 5 nm gold QDs bound within the pores of the 3-nm-pore crystalline template. Occupied rings show the QDs (dark areas) are surrounded and held in place by the chaperonin pores. Empty rings have a brighter, less electron-dense appearance. We are currently investigating why some sites are unoccupied. We suspect that this is related to the solvent accessibility of thiols on the apical loops, or to the size variation of the 5 nm QDs. **d**, Ordered region of 10 nm gold bound to a 9-nm-pore template with similar area coverage as in **c**. The chaperonins are occluded by the 10 nm QDs.

formed chaperonins that assembled into disk-shaped, hexagonally packed 2D crystals of up to 20 μm in diameter (Fig. 2a,b). The order within the crystalline lattices is illustrated by fast Fourier transformation of the TEM images (Fig. 2b, inset) which produced an optical diffractogram expressing the periodicity.

To determine whether the thiol-containing 2D crystals of chaperonins could act as templates to bind and order nanoparticle QDs into arrays, we initially used commercially available gold QDs of different diameters (Fig. 3). The uniform dispersion of these gold QDs in aqueous solution allows them to bind to hydrated chaperonin templates. To increase their likelihood of binding specifically to the reactive thiol of the cysteines, however, we passivated the gold particles with the ligand bis(*p*-sulphonatophenyl)phenylphosphine (BSPP)[35]. BSPP displaces the citrate shell formed during synthesis of gold QDs[36], and thereby reduces non-specific binding of the QDs to the protein template. The passivated gold QDs were reacted with the chaperonin templates attached to formvar-coated TEM grids (see Methods) and imaged in TEM mode at 60 kV. At low magnifications, the chaperonin 2D crystals were visualized in the TEM using the electron density of the gold QDs themselves (Fig. 3a). At high magnification, the chaperonin–gold interactions were visualized in the TEM by negative-staining of the samples with uranyl acetate (Fig. 3b–d). Individual chaperonins in solution were observed to bind gold QDs on one or both ends. The QDs are presumably held in place by multiple dative bonds formed between the gold surface and the thiols within the pores (Fig. 3b, inset).

In control experiments, using chaperonin 2D crystals without exposed cysteines and with or without deletions of the the amino acid loop, the gold QDs appeared randomly distributed with no specific binding to the chaperonin crystals. On the surface of chaperonin 2D crystals with cysteines, however, the gold QDs bound specifically onto the pores (Fig. 3c), forming regions of order on the protein (Fig. 3d) separated from one another by the cracked regions that resulted from drying, indicating that the engineered chaperonin crystals function as templates for gold QDs in solution. These chaperonin templates were size-selective when attached to substrates and appeared to bind QDs only on the exposed side. Templates made from beta mutants with cysteines added to the apical loop that formed 3 nm rings of reactive thiols, ordered 5 nm (± 3 nm) gold QDs, but did not order 10 nm (± 2 nm) or 15 nm (± 1 nm) gold QDs, which bound randomly on the template surface. (Variations in size distribution of gold QDs are a result of the manufacturer's method of synthesis.) The chaperonin templates with the loop removed and cysteines on the apical domains that formed 9 nm rings of reactive thiols, ordered 10 nm (± 2 nm) gold QDs, but 5 nm (± 3 nm) and 15 nm (± 1 nm) QDs bound randomly. This size selectivity

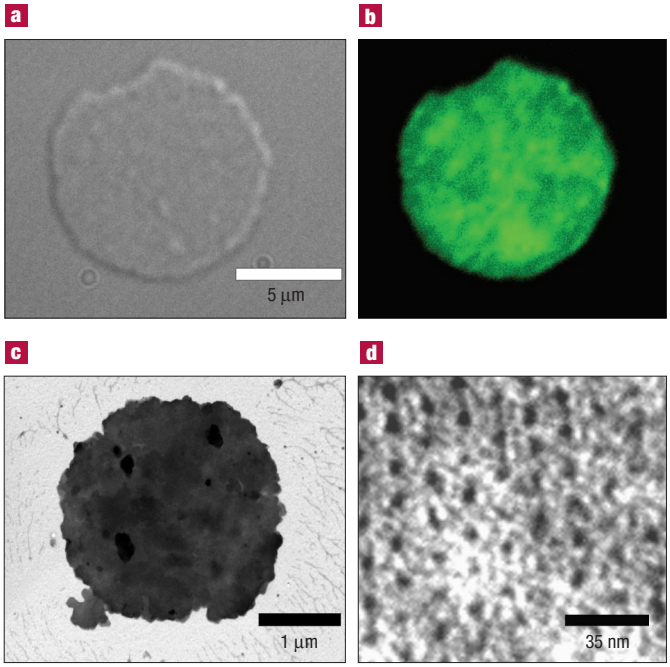

Figure 4 Semiconductor QD arrays. a, DIC light micrograph of an 8 μm crystalline disc of the 3-nm-pore template with bound 4.5 nm luminescent CdSe–ZnS QDs. **b**, Both dry and rehydrated arrays fluoresced indicating the QDs bound to the template. 2D crystals of a beta variant without added cysteines showed minimal QD binding (see Supplementary Information). **c**, Low-magnification TEM of an unstained array of CdSe–ZnS QDs. Image contrast is due to the bound semiconductor QDs. **d**, Higher-magnification image of the same crystal showing an ordered region of QDs bound to the chaperonin lattice.

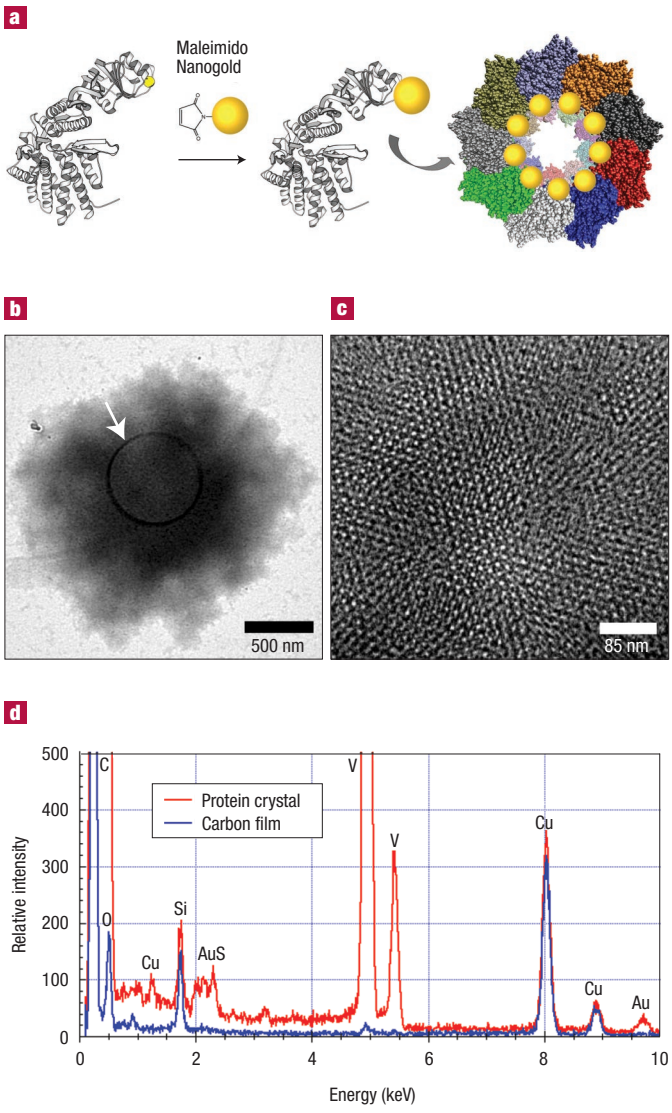

Figure 5 Chaperonin subunit mediated self-assembled Nanogold arrays. a, Covalent attachment of 1.4 nm monomaleimido Nanogold to subunits of the 9-nm-pore beta chaperonin variant through Michael addition of cysteine thiol to QD surface maleimide groups. Right: The possible arrangement of nine 1.4 nm covalently attached Nanogold QDs viewed at one end of a ring assembled from the derivatized subunit. **b**, Low-magnification TEM image of a 2D crystalline array lightly stained with methylamine vanadate. Heavy atom stains were avoided to enable imaging of the tiny Nanogold particles. The dark circular feature (arrowed) is the result of polymerization of mobile hydrocarbon attracted to the periphery of the electron beam and shows the area analyzed corresponding to the red spectrum in **d**. **c**, Higher-magnification bright-field EFTEM image of the array revealing the ordered pattern of electron density that extends across the crystalline template. **d**, XEDS spectra of bare carbon film (blue) and Nanogold array (red) from the probe outlined in **b**. Characteristic X-ray peaks from gold (Au M_α ~2 keV and Au L_α ~9.7 keV) confirm the presence of Nanogold within the array and the relative absence of Au on the support film away from the Nanogold array.

is due to the accessibility and positioning of cysteine residues within the pores of the templates.

The precision of the centre-to-centre spacing of gold QDs ordered by the chaperonin templates was 16 nm (± 2 nm, over 200 measurements) for both 5 and 10 nm gold QD arrays, as determined by TEM. This is consistent with the centre-to-centre spacing of the chaperonin pores in the underlying templates. The edge-to-edge spacing between QDs ranged from 6 to 10 nm for arrays made with 5 nm (± 3 nm) QDs bound to 3-nm-pore chaperonin templates and from 4 to 6 nm for arrays made with 10 nm (± 2 nm) QDs bound to 9-nm-pore chaperonin templates. We attribute this variation in spacing to both the variation in the size of the gold QDs and to imperfections in the lattice of the chaperonin templates resulting from drying, cracking and dislocations within the arrays. The observed variation in QD spacing could be decreased with improved routes to QD synthesis having narrower size distributions. With QDs that are more monodisperse, the precision of centre-to-centre spacing in our gold arrays should make it possible to tune the physical properties of the arrays by controlling the interparticle coupling using QDs of different sizes[37].

To investigate whether chaperonin templates could bind and order semiconductor QDs, we used 4.5 nm luminescent core–shell CdSe–ZnS QDs[38]. These QDs were reacted with 3-nm-pore chaperonin templates attached to glass or formvar substrates. Semiconductor QDs have low solubility in aqueous solutions. A QD suspension in trioctylphosphine/trioctylphosphine oxide (TOP/TOPO) diluted with butanol was reacted with dried chaperonin templates. Under these conditions the QDs bound to the cysteine-containing chaperonin templates (Fig. 4), but not appreciably to chaperonin 2D crystals without exposed cyteines (see Supplementary Information). This is consistent with observations that Zn in the outer ZnS shell of CdSe–ZnS QDs binds solvent-exposed thiols[39].

The differential interference contrast (DIC) image of the QD-bound template (Fig. 4a) and the corresponding fluorescent image

(Fig. 4b) reveal that QDs bound to cysteine thiol retain their luminescent properties[40]. The mottled appearance of both the QD luminescence and the electron density of low-magnification TEM images indicate that the QDs are unevenly distributed on the chaperonin templates (Fig. 4b,c). At higher magnification of unstained samples, regions of ordered QDs are visible (Fig. 4d). These regions are separated by unoccupied regions where QDs did not bind to the protein template. We did not determine whether this difference was due to drying or to solvent effects of the butanol, both of which may alter the structure of the chaperonin template and the accessibility of the thiols. We did observe that water-soluble (silica-capped) CdSe–ZnS[41] QDs containing exposed thiol groups bound more uniformly to hydrated chaperonin templates. The thiols on these QDs, however, caused them to aggregate, forming defective arrays.

To determine whether QDs could be manoeuvered into arrays by first tethering them to beta subunits and then ordered as the subunits assemble into chaperonins and 2D crystals, we used commercially available 1.4 nm gold QDs derivatized with surface-accessible, thiol-reactive maleimide groups (monomaleimido Nanogold). These Nanogold QDs were covalently bound to the mutant beta subunit with cysteine inserted in place of the 28-amino-acid loop in the apical domain (Fig. 5). Subunits, with Nanogold attached, assembled into chaperonins in the presence of ATP/Mg^{2+} (Fig. 5a); these chaperonins formed 2D crystals (Fig. 5b, c). The binding of the Nanogold QDs and localization within the pores of the chaperonin crystals was confirmed by analytical TEM (Figs 5,6).

Ordered hexagonally spaced inclusions within the crystalline template were observed and determined to contain gold by imaging methylamine vanadate-stained Nanogold samples in bright-field energy-filtering (EFTEM) mode and by using X-ray energy dispersive spectroscopy (XEDS) (Fig. 5b–d). Oxygen plasma-treated carbon support films were used because they are more stable in an electron beam than formvar. Because the protein templates do not adhere to plasma-treated carbon as well as they do to formvar, samples were stained with methylamine vanadate to enable identification of their location on the substrate. The XEDS spectrum of the Nanogold array reveals distinct peaks due to gold that are well separated from vanadium and copper peaks from the stain and carbon/copper support respectively (Fig. 5d).

High-angle annular dark-field (HAADF) scanning transmission electron microscopy (STEM) was used to image the gold localized and ordered within the Nanogold arrays (Fig. 6). Comparisons of bare Nanogold to Nanogold ordered into an array revealed that multiple Nanogold QDs were localized within the pores of the crystallized chaperonins (Fig. 6a,b). The HAADF image of the Nanogold crystal also confirms the presence of gold within the chaperonin pores because contrast in HAADF imaging mode is dependent on atomic number, and nearly independent of focus or thickness. A HAADF comparison of the diameter of bare Nanogold particles on carbon to the diameter of the gold nanoparticles contained within the central pores of the chaperonins that template the Nanogold into arrays, reveals that the central diameters are approximately eight to twelve times that of the diameter of a single Nanogold QD. This observation is consistent with our model, which suggests that each ring can contain up to nine Nanogold QDs (one per subunit). A lower magnification HAADF image of a similar area of an array reveals that the ordering of the gold extends throughout the template (Fig. 6c). High-resolution XEDS mapping attempts of the gold within the array were unsuccessful because the crystals were destroyed with the electron dose needed for such measurements. Electron energy loss spectroscopy mapping using the Au–O shell was correspondingly unsuccessful because the V–M shell edge lies in close proximity to the Au–O shell and thus masks the gold signal.

Crystal thickness measurements (by atomic force microscopy and TEM) suggest that these crystals can be multilayered (see Supplementary Information), and we have observed crystals ranging from one to five layers (approximately 20 to 200 nm) thick (R. M. Stevens *et al.* unpublished results). The size limit of nanoparticles that can be assembled by chaperonin subunits into arrays and the physical consequences of their close packing have yet to be determined. The assembly of QDs into arrays by first covalently attaching them to subunits may create more defect-tolerant arrays, because each chaperonin is composed of 18 subunits and therefore there are 18 chances for each site in the array to contain at least one QD. Likewise, the regions of QD ordering within arrays assembled this way appear to span the dimensions of the crystalline template and with fewer defects than previously observed. These types of arrays may find use in applications that demand longer range ordering than the 5 and 10 nm gold and semiconductor nanoparticle binding protocols allow.

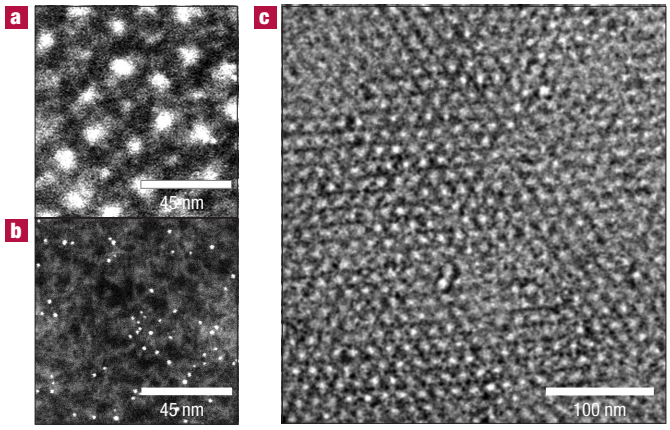

Figure 6 HAADF STEM imaging of Nanogold arrays. a, The diameter of the features contributing to the array periodicity is consistent with multiple QDs localized within each chaperonin ring. The diameter of electron density observed within the rings forming the array in **a** is approximately 8 to 12 times that observed for single 1.4 nm Nanogold QDs (**b**). **c**, The periodicity from the Nanogold QDs localized within the rings extends across the entire crystal forming the ordered array.

Our results show that a hybrid bio/inorganic approach to nanophase materials organization is possible and that, to this end, the functionality of proteins can be rationally engineered. Using structural information and recombinant biotechnology techniques, we demonstrate that genetically engineered chaperonins can function both as templates and as vehicles for controlled nanoscale organization of preformed QDs into ordered arrays. A next step in this research project is to wire these arrays together into functional devices. This may also be done using genetics, because alternative binding sites may be engineered at different locations on the chaperonin.

Future directions involve the possibility to induce asymmetry within the arrays by engineering alternative facets of the protein crystal. With advances in microbial genetics, for example using phage and cell surface display to identify inorganic binding peptide sequences[42], the usefulness of this system may be extended beyond soft metals to the recognition of other materials by the addition of sequences back into the loop region that was removed. This is a plausible research scenario given the plasticity within the apical loop region of the thermophilic chaperonin. The genetic flexibility and structural versatility of chaperonins suggests that these proteins have a place among other self-assembling biomolecules as tools for the development of nanotechnology. These developments will be expedited by combining the 'soft' organic biological sciences with the 'hard' inorganic materials sciences.

METHODS

MODELS

A homology model for *S. shibatae* HSP60beta was made using the web-based service Swiss Model (http://www.expasy.ch/swissmod/SWISS-MODEL.html). Seven PDB entries of solved structures of homologous proteins were used as templates scoring between 48% and 64% sequence identity in pairwise alignment with native *S. shibatae* beta. The structure was relaxed *in vacuo* with the GROMOS96 force field. Symmetry operations were applied to the subunit to form nine-fold symmetrical rings that were assembled into 18-mer chaperonins. All models were constrained by dimensions observed for different chaperonin views as measured in the TEM.

GENETIC MODIFICATIONS

A standard polymerase chain reaction mutagenesis method as described previously[43] was followed to introduce cysteine residues and to delete the portions of DNA coding for the apical loop. All mutant subunits were purified as described in the text and in corresponding references.

CHAPERONIN ASSEMBLY AND CRYSTALLIZATION

Chaperonins were assembled from purified subunits with the concomitant formation of 2D crystals in solution, without the need for an interacting interface. Concentrated stock solutions of ATP and $MgCl_2$ (both from Sigma, St. Louis, Missouri) were added to purified subunits of 1.5 mg ml^{-1}, 25 μM in 25 mM HEPES (Fisher Biotechnology, Fairlawn, New Jersey) 3.5 mM TCEP (Hampton Research, Laguna Niguel, California) such that the final ATP concentration was 4 mM and the final $MgCl_2$ concentration was 10 mM. The crystallization solution was incubated at 4 °C overnight, after which crystals were observed as a white precipitate.

QD ARRAY FORMATION

For gold QD binding, crystalline protein templates were applied to formvar-coated 200 mesh copper TEM grids and gold QDs (Ted Pella, Redding, California) were bound by floating the sample side of the grid on 5 μl drops of passivated QD sols, wicking away with filter paper and washing by floating on HAT buffer—25 mM HEPES, 0.1% sodium azide (Sigma, as above), 3 mM TCEP, pH 7.5—for 10 minutes. This process was repeated up to 10 times as more applications increased the site occupation on the template. However, the trade-off was that the shear forces created by wicking away the QDs sometimes disrupted the underlying protein template. The 10 nm gold QDs bound better with fewer applications than the 5 nm QDs, and after 10 applications the 3-nm templates were considerably broken up. Samples were viewed in a LEO 912 AB TEM at 60 kV. All quantitative image analysis was performed using AnalySIS 3.5 (Soft Imaging System, Lakewood, Colorado).

Semiconductor QDs were bound and imaged in a similar manner to gold QDs with the exception that templates were applied to TEM grids, washed with water, dried and re-swelled with butanol before QD binding. For light microscopy, the crystals were applied to a formvar-coated glass slide, rinsed with water, dried, rinsed with butanol, and covered with a coverslip. A dilute slurry of CdSe–ZnS QDs in TOP/TOPO/butanol was passed over the crystals by capillary action and thoroughly rinsed with butanol, and imaged in bright-field, DIC and fluorescence modes on a Leica DMR/X microscope.

Nanogold arrays were fabricated in the following manner. Subunits of the loopless mutant with the cysteine insertion were reacted with an excess of Nanogold (monomaleimido Nanogold, Nanoprobes, Yaphank, New York) as per the instructions supplied by the manufacturer. The Nanogold-tagged subunits were separated from unreacted protein and excess Nanogold using gel filtration chromatography (BioRad BioGel P-10, Hercules, California), concentrated to 1.5 mg ml^{-1} and assembled into rings and 2D crystals as described above.

ANALYTICAL ELECTRON MICROSCOPY (AEM) MEASUREMENTS

Samples were applied to carbon-coated grids (Ted Pella, Redding, California) that were briefly treated with an oxygen plasma to enhance protein adhesion to carbon. Specimens were analysed at room temperature using a double-tilt Be stage in a FEI TecnaiF20 AEM. The instrument was operated in the TEM, STEM, HAADF EFTEM modes at 200 kV using a Schottky field-emisson gun electron source. All XEDS measurements were made using an EDAX ultrathin window Si(Li) detector having a full width at half maximum of ~150 eV at Mn K_α. Energy filtering and electron spectroscopy was accomplished using a Gatan GIF2000 imaging electron energy loss spectrometer. Nominal probe sizes used during the study varied between 0.5–500 nm depending upon the nature of the measurements or observations.

Received 19 August 2002; accepted 25 October; published 24 November 2002.

References

1. Zhirnov, V. V. & Herr, D. J. C. New frontiers: Self-assembly and nanoelectronics. *Computer* **34,** 34–43 (2001).
2. Xia, Y., Gates, B., Yin, Y. & Lu, Y. Monodispersed colloidal spheres: Old materials with new applications. *Adv. Mater.* **12,** 693–713 (2000).
3. Sato, T., Ahmed, H., Brown, D. & Johnson, B. F. G. Single electron transistor using a molecularly linked gold colloidal particle chain *J. Appl. Phys.* **82,** 696–701 (1997).
4. Nalwa, H. S. *Handbook of Materials and Nanotechnology* (Academic, San Diego, 2000).
5. Likharev, K. K. Single electron devices and their applications. *Proc. IEEE* **87,** 606–632 (1999).
6. Thelander, C. *et al.* Gold nanoparticle single-electron transistor with carbon nanotube leads. *Appl. Phys. Lett.* **79,** 2106–2108 (2001).
7. Maier, S. A. *et al.* Plasmonics - A route to nanoscale optical devices. *Adv. Mater.* **13,** 1501–1505 (2001).
8. Maier, S. A., Brongersma, M. L., Kik, P. G. & Atwater, H. A. Observation of near-field coupling in metal nanoparticle chains using far-field polarization spectroscopy. *Phys. Rev. B* **65,** 193408 (2002).
9. Zrenner, A. *et al.* Coherent properties of a two-level system based on a quantum-dot photodiode. *Nature* **418,** 612–614 (2002).
10. Berven, C. A., Clarke, L., Mooster, J. L., Wyborne, M. N. & Hutchison, J. E. Defect-tolerant single-electron charging at room temperature in metal nanoparticle decorated biopolymers. *Adv. Mater.* **13,** 109–113 (2001).
11. Park, M., Chaikin, P. M., Register, R. A. & Adamson, D. H. Large area dense nanoscale patterning of arbitrary surfaces. *Appl. Phys. Lett.* **79,** 257–259 (2001).
12. Hulteen, J. C. & Duyne, R. P. V. Nanosphere lithography: A materials general fabrication process for periodic particle array surfaces. *J. Vac. Sci. Technol. A* 1553–1558 (1995).
13. Richter, J. *et al.* Nanoscale palladium metallization of DNA. *Adv. Mater.* **12,** 507–510 (2000).
14. Keren, K. *et al.* Sequence-specific molecular lithography on single DNA molecules. *Science* **297,** 72–75 (2002).
15. Sleytr, U. B., Messner, P., Pum, D. & Sara, M. Crystalline bacterial cell surface layers (s layers): From supramolecular cell structure to biomimetics and nanotechnology. *Angew. Chem. Int. Edn* **38,** 1034–1054 (1999).
16. Douglas, K., Clark, N. A. & Rothschild, K. J. Nanometer molecular lithography. *Appl. Phys. Lett.* **48,** 676–678 (1986).
17. Hall, S. R., Shenton, W., Engelhardt, H. & Mann, S. Site-specific organization of gold nanoparticles by biomolecular templating. *Chem. Phys. Chem.* **3,** 184–186 (2001).
18. Shenton, W., Douglas, T., Young, M., Stubbs, G. & Mann, S. Inorganic-organic nanotube composites from template mineralization of tobacco mosaic virus. *Adv. Mater.* **11,** 253–256 (1999).
19. Douglas, T. & Young, M. Virus particles as templates for materials synthesis. *Adv. Mater.* **11,** 679–681 (1999).
20. Douglas, T. & Young, M. Host-guest encapsulation of materials by assembled virus protein cages. *Nature* **393,** 152–155 (1998).
21. Wang, Q., Lin, T., Tang, L., Johnson, J. E. & Finn, M. G. Icosahedral virus particles as addressable nanoscale building blocks. *Angew. Chem. Int. Edn* **41,** 459–462 (2002).
22. Lee, S. W., Mao, C., Flynn, C. E. & Belcher, A. M. Ordering of quantum dots using genetically engineered viruses. *Science* **296,** 892–895 (2002).
23. Yamashita, I. Fabrication of a two-dimensional array of nano-particles using ferritin molecule. *Thin Solid Films* **393,** 12–18 (2001).
24. Hartl, F. U. & Hayer-Hartl, M. Molecular chaperones in the cytosol: From nascent chain to folded protein. *Science* **295,** 1852–8 (2002).
25. Trent, J. D., Kagawa, H. K., Yaoi, T., Olle, E. & Zaluzec, N. J. Chaperonin filaments: The archaeal cytoskeleton? *Proc. Natl. Acad. Sci. USA* **94,** 5383–5388 (1997).
26. Ellis, M. J. *et al.* Two-dimensional crystallization of the chaperonin TF55 from the hyperthermophilic archaeon *Sulfolobus solfataricus. J. Struct. Biol.* **123,** 30–36 (1998).
27. Kagawa, H. K. *et al.* The 60 kDa heat shock proteins in the hyperthermophilic archaeon *Sulfolobus shibatae. J. Mol. Biol.* **253,** 712–25 (1995).
28. Ditzel, L. *et al.* Crystal structure of the thermosome, the archaeal chaperonin and homolog of CCT. *Cell* **93,** 125–38 (1998).
29. Xu, Z., Horwich, A. L. & Sigler, P. B. The crystal structure of the asymmetric groEL-groES-(adp)7 chaperonin complex. *Nature* **388,** 741–50 (1997).
30. Koeck, P. J. B., Kagawa, H. K., Ellis, M. J., Hebert, H. & Trent, J. D. Two-dimensional crystals of reconstituted β–subunits of the chaperonin TF55 from *Sulfolobus shibatae. Biochim. Biophys. Acta* **1429,** 40–44 (1998).
31. Schoehn, G., Quaite-Randall, E., Jimenez, J. L., Joachimiak, A. & Saibil, H. R. Three conformations of an archaeal chaperonin, TF55 from *Sulfolobus shibatae. J. Mol. Biol.* **296,** 813–819 (2000).
32. Peitsch, M. C. Protein modeling by e-mail. *Bio/Technology* **13,** 658–660 (1995).
33. Guex, N. & Peitsch, M. C. Swiss-model and the swiss-pdbviewer: An environment for comparative protein modelling. *Electrophoresis* **18,** 2714–2723 (1997).
34. Guex, N., Diemand, A. & Peitsch, M. C. Protein modelling for all. *Trends Biochem. Sci.* **24,** 364–367 (1999).
35. Loweth, C. J., Caldwell, W. B., Peng, X., Alivisatos, A. P. & Schultz, P. G. DNA-based assembly of gold nanocrystals. *Angew. Chem. Int. Edn* **38,** 1808–1812 (1999).
36. Novak, J. P., Nickerson, C., Franzen, S. & Feldheim, D. L. Purification of molecularly bridged metal nanoparticle arrays by centrifugation and size exclusion chromatography. *Anal. Chem.* **73,** 5758–5761 (2001).
37. Dujardin, E. & Mann, S. Bio-inspired materials chemistry. *Adv. Mater.* **14,** 775–788 (2002).
38. Dabbousi, B. O. *et al.* (CdSe)ZnS core-shell quantum dots: Synthesis and characterization of a size series of highly luminescent nanocrystallites. *J. Phys. Chem. B* **101,** 9463–9475 (1997).
39. Chan, W. C. & Nie, S. Quantum dot bioconjugates for ultrasensitive nonisotopic detection. *Science* **281,** 2016–2018 (1998).
40. Bruchez, M. Jr., Moronne, M., Gin, P., Weiss, S. & Alivisatos, A. P. Semiconductor nanocrystals as fluorescent biological labels. *Science* **281,** 2013–2016 (1998).
41. Gerion, D. *et al.* Synthesis and properties of biocompatible water-soluble silica-coated semiconductor nanocrystals. *J. Phys. Chem. B* **105,** 8861–8871 (2001).
42. Whaley, S. R., English, D. S., Hu, E. L., Barbara, P. F. & Belcher, A. M. Selection of peptides with semiconductor binding specificity for directed nanocrystal assembly. *Nature* **405,** 665–668 (2000).
43. *Current Protocols in Molecular Biology* (eds Ausubel, F. M. *et al.*) (Wiley, New york, 1998).

Acknowledgements

The authors thank A. P. Alivisatos and W. J. Parak for the semiconductor quantum dots, M. Wilson and Y. F. Li for assistance in assembling chaperonin models, A. Madhukar for quantum dot discussions, and R. Boyle and J. Varelas of the NASA BioVis Center for use of the LEO TEM. This work was supported through funding from the NASA Ames Center for Nanotechnology. We also acknowledge funding from the US Department of Energy, the Defense Advanced Research Projects Agency, and the NASA Ames Director's Discretionary Fund. Work at ANL was supported in part by the US DoE BES-MS W-31-109-Eng-38.

Correspondence and requests for materials should be addressed to R.A.M. or J.D.T.

Supplementary Information accompanies the paper on the website for *Nature Materials* (http://www.nature.com/naturematerials)

Competing financial interests

The authors declare that they have no competing financial interests.